95171

CHARACTERISTICS OF FAULTS IN NONWELDED IGNIMBRITES FROM THE PAJARITO PLATEAU AND IMPLICATIONS FOR FLUID FLOW

by

Jennifer E. Wilson

Submitted in Partial Fulfillment
of the Requirements for the

Doctorate of Philosophy in Geology

New Mexico Institute of Mining and Technology
Department of Earth and Environmental Science

Socorro, New Mexico

December, 2004

14674

TABLE OF CONTENTS

Page

Title Page..... i

Abstract

Acknowledgments..... ii

Table of Contents..... iii

List of Figures..... ix

List of Tables..... xiv

Chapter 1: Introduction..... 1

Background..... 1

Organization of Dissertation..... 7

Chapter 2: Petrophysical and Mechanical Characteristics of Ignimbrites..... 9

Chapter 3: Deformation Bands in Nonwelded Ignimbrites: Petrophysical Controls on Fault-Zone Deformation and Evidence of Preferential Fluid Flow..... 13

Abstract..... 13

Introduction..... 14

Study Sites..... 17

Bandelier Tuff, Los Alamos, New Mexico..... 17

Calico Hills & Topopah Spring Tuffs, Busted Butte, Nevada..... 17

Methods..... 18

Fault-Zone Structures in Ignimbrites..... 19

Fractures Versus Deformation Bands..... 19

Alteration and Mineralization..... 23

Mode of Failure Transition..... 24

Discussion..... 25

Controls on Fault-Zone Structure in Ignimbrites..... 25

Implications for Fluid Flow..... 27

Conclusions..... 28

Acknowledgments..... 29

References Cited..... 29

Chapter 4: Diagenetic Alteration and Mineralization of Deformation-Band Faults in the Bandelier Tuff, Los Alamos, New Mexico: A Record of Vadose-Zone Flow and Transport..... 33

Abstract..... 33

Introduction..... 34

Geologic Setting..... 38

Methods..... 40

Outcrop Characterization, Petrography, and Microprobe Analyses.... 40

Bulk Mineralogy (XRD)..... 43

Whole Rock Geochemistry (XRF & INAA)..... 44

Stable Isotope Characterization..... 45

Results..... 46

Outcrop Character and Petrography of Protolith-Deformation Band Sets..... 46

Mineralogy and Whole Rock Geochemistry of Protolith-Deformation Band Sets..... 54

Chemical Compositions of Protolith Matrix, Mafic Minerals, and Fault-Zone Smectite..... 59

Rare-Earth Element (REE) Distributions of Deformation Bands and Protolith..... 63

Stable Isotope Characterization of Deformation Bands and Adjacent Protolith..... 68

Discussion..... 69

Oxygen Isotope Enrichment..... 69

The Origin of Smectite in Deformation Bands..... 71

Calcite Cementation in Deformation Bands..... 74

Oxide Mineralization within a Unique Deformation-Band Fault Zone 75

Mineralogical Differences Between Deformation Bands and Protolith Attributed to Protolith Variations: Implications for Deformation-Band Propagation and Origin in Ignimbrites..... 76

Geochemical Differences between Deformation Bands and Protolith Attributed to Preferential Solute Transport..... 78

Proposed Model of Structural and Diagenetic Evolution of Deformation Bands in Nonwelded Bandelier Tuff..... 80

Implications for Vadose-Zone Fluid Flow and Transport in the Bandelier Tuff..... 82

Conclusions..... 86

Acknowledgments..... 87

References..... 88

Chapter 5: Saturated Permeability of Deformation-Band Fault Zones in Nonwelded Ignimbrites of the Bandelier Tuff..... 95

Abstract..... 95

Introduction..... 96

Geologic Setting..... 101

Characteristics of Deformation-Band Faults on the Pajarito Plateau.. 104

Methods..... 106

Standardization..... 108

Results..... 109

Evaluation of Approaches to Determining Porosity..... 109

Standardization of Saturated Permeability Measurements..... 109

Porosity and Permeability Differences for Protolith-Fault Pairs..... 112

Permeability Ranges for All Protoliths and Faults..... 114

Discussion..... 115

Measurement Error..... 115

Non-Darcian Flow Effects..... 116

Effect of Deformation-Band Thickness on Permeability Measurements..... 117

Uncertainties in Saturated Permeabilities Associated with Smectite and Calcite in Deformation Bands..... 118

Heterogeneity of Saturated Permeabilities of Protolith Versus Deformation Bands..... 119

Implications for Groundwater Flow Through Ignimbrites..... 119

Conclusions..... 122

Acknowledgments..... 123

References..... 123

Chapter 6: Conclusion..... 128

Suggestions for Future Work..... 130

Image Analysis..... 130

Detailed Petrographic and Geochemical Characterization of Nonwelded Ignimbrite Units..... 131

3-D Imaging of Pore Space and Flow (Unsaturated and Saturated)... 132

Additional Saturated Permeability Measurements of Fault-Protolith Pairs..... 132

Determine Spatial Distribution of Deformation Bands by Detailed Mapping of the Bandelier Tuff..... 133

Similar Investigations in Other Ash-Dominated Ignimbrite Deposits 133

Deformation Experiments and Subsequent Investigation of Fault-Zone Structures in Nonwelded Ignimbrites..... 134

Appendix A: Outcrop Characterization of Small-Displacement Faults and Corresponding Protolith in the Bandelier Tuff (NM) and Calico Hills Tuff (NV)..... 135

Location and Description of Small-Displacement Faults Investigated in the Bandelier Tuff, Pajarito Plateau, New Mexico..... 135

Location and Description of Small-Displacement Faults Investigated in the Calico Hills Tuff, Busted Butte, Nevada..... 143

Appendix B: Sample Preparation and Petrographic Data Collection..... 153

Epoxy-Impregnation Procedure..... 153

Petrographic Point Count Determinations..... 154

Porosity Determinations..... 157

Textures of Fault-Zone Material and Corresponding Protolith Observed in Back-Scattered Electron and Secondary Electron Microprobe Imaging.... 162

Appendix C: Hydrologic Data Collection..... 164

Construction and Use of Air-Minipermeameter..... 164

Procedure Followed for Field and Laboratory Measurement of Air Permeability..... 165

Calculation of Permeability..... 166

Source of Input Variables..... 168

Corrections to Input Variables..... 168

Calibration of Flow Gauges..... 169

Calibration of Pressure Gauges..... 170

Permeability Data for all Samples/Outcrop Locations..... 172

References Cited..... 184

CHAPTER 5

SATURATED PERMEABILITY OF DEFORMATION-BAND FAULT ZONES IN NONWELDED IGNIMBRITES OF THE BANDELIER TUFF[1]

Abstract

Faults can impact recharge, groundwater flow, and solute transport by modifying fluid pathways in the subsurface. Both isolated, major fault zones and more numerous small-displacement faults may affect these hydrologic processes. However, most models of groundwater flow incorporate only large fault zones. Our study focuses on much more common, small-displacement faults across the Pajarito Plateau of northern New Mexico, in the ash-dominated nonwelded ignimbrites of the Bandelier Tuff. These faulted ignimbrites contain perched aquifers, one of the primary groundwater flow regimes beneath the Pajarito Plateau. In contrast to low porosity and crystalline rocks, which fail along shear fractures, nonwelded ignimbrites can deform by grain crushing and pore collapse within deformation bands. Unlike fractures, which increase saturated permeability through welded ignimbrites by at least two orders of magnitude, we show that deformation bands reduce nonwelded ignimbrite saturated permeability by at least an order of magnitude.

Because deformation bands are very narrow, the volume interrogated by our air-minipermeameter includes protolith. In addition, measurements made with an air-

[1]To be submitted to Water Resources Research.

minipermeameter cannot take into account the impact of swelling clays like smectite, which is common in these faults, on permeability. Thus, our permeability values represent maximum estimates, and the permeability reduction associated with faults is likely to be greater than we report. If these differences exceed the range in permeability exhibited by unfaulted ignimbrite, deformation bands may affect saturated flow by introducing effective permeability heterogeneity and/or anisotropy into permeable nonwelded units. These permeability variations, even if relatively small, may be important at production time scales, possibly impacting recovery rates from perched aquifers in stratigraphically lower units of the Bandelier Tuff.

Introduction

Saturated flow is affected by the hydrologic properties of subsurface geologic features. Where subsurface lithologic units are faulted, fluid flow pathways can be modified by either juxtaposition of units with different hydrologic properties and/or processes that change the permeability of the fault zone itself, such as deformation, alteration, and cementation [e.g., Knipe, 1993; Caine et al., 1996; Rawling et al., 2001]. For faults in which displacement is less than bed thickness, the only significant impact on flow will be produced by structural and diagenetic modification of the fault zone. Such faults are the focus of this study of ash-dominated ignimbrite deposits.

Ignimbrites are spatially heterogeneous pyroclastic flow deposits consisting of poorly sorted assemblages of phenocrysts, pumice, and lithic fragments in a matrix of glass shards and ash. Individual cooling units within these deposits show a range in degree of welding (compaction and fusion of matrix glass and pumice) and postdepositional crystallization, including devitrification of volcanic glass to cristobalite

and feldspar, and/or vapor-phase crystallization of minerals such as tridymite and feldspar from vapors in pore spaces. This range reflects variations in eruption temperature, the mechanics of deposition, entrainment of volatiles, distance from caldera source, and composition [e.g., Smith and Bailey, 1966].

For hydrologic purposes, three categories of ignimbrite unit are considered, each of which has distinct ranges of porosity and permeability. Welded ignimbrites have low porosities (10-13%) [Wilson et al., 2003] and permeabilities (10^{-19} to 10^{-15} m^2) [Tidwell and Wilson, 1999; Wohletz, 1999]. Crystallized nonwelded ignimbrites have intermediate porosities relative to the other two categories (21-51%) [Wilson et al., 2003] and variable permeabilities (10^{-16} to 10^{-12} m^2) [Rogers and Gallaher, 1995; Springer and Schofield, 2002]. Glassy nonwelded ignimbrites have high porosities (32-56%) [Wilson et al., 2003] and variable permeabilities (10^{-16} to 10^{-12} m^2) [Winograd and Thordarson, 1975; Istok et al., 1994; Rogers and Gallaher, 1995; LeCain, 1997; Springer and Schofield, 2002]. Undeformed and uncompacted pumice and matrix glass shards are responsible for the high porosities observed in nonwelded ignimbrite units. The heterogeneity of clast contacts and the resulting variability of pore throat geometries is the likely cause of the highly variable saturated permeabilities documented in nonwelded units.

Hydrologic properties can be linked to controls on deformation in these different ignimbrite units. Wilson et al. [2003] have shown that for ash-dominated ignimbrites of Los Alamos, New Mexico, and Busted Butte, Nevada, welded units deform by fracture, glassy nonwelded units deform by cataclasis within deformation bands (Fig. 5.1), and crystallized nonwelded units deform by either of these mechanisms, depending on the

degree and nature of postdepositional crystallization. High porosity and permeability are generally correlated to low grain-contact area and strength, which facilitate fault-zone failure by cataclasis within deformation bands. These narrow zones in which grain crushing, grain-boundary sliding, and pore collapse accommodate mm-cm displacement are only found in nonwelded units. Low porosity and permeability typically reflect high

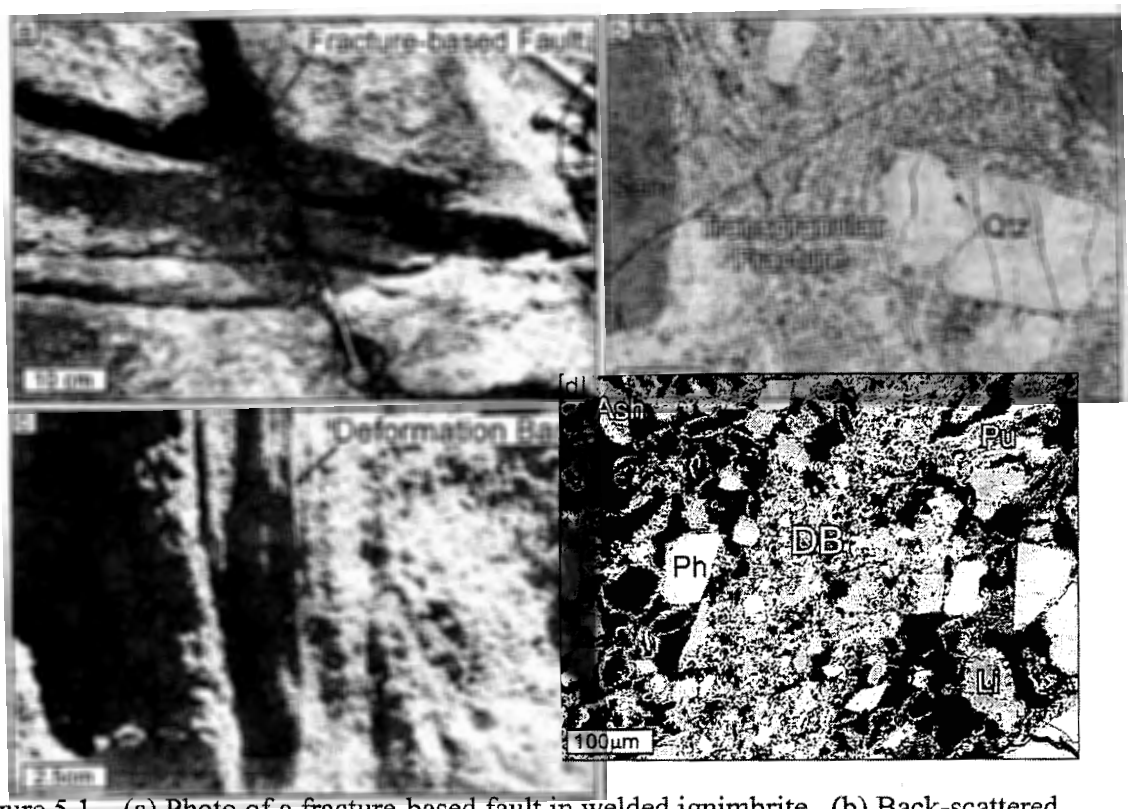

Figure 5.1. (a) Photo of a fracture-based fault in welded ignimbrite. (b) Back-scattered electron (BSE) image of a transgranular fracture in welded ignimbrite. Phenocrysts of sanidine (San) and quartz (Qtz) in a welded fabric of flattened pumice are crosscut by an open transgranular fracture. The fracture can be considered a plane of increased porosity (black) and pore connectivity. (c) Outcrop photo of 1 mm-wide deformation bands in nonwelded ignimbrite. (d) BSE image of a deformation band (DB), characterized by reduced pore- and grain-size relative to protolith. Ph = phenocryst, Pu = pumice, and Li = lithic clast.

grain-contact area and strength, which lead to fault-zone failure by fracture in welded and some crystallized nonwelded ignimbrites [Wilson et al., 2003].

Similar material controls on deformation are demonstrated by other field-based studies in different lithologies. Low porosity sedimentary and crystalline rocks deform by fracture [e.g., Chester and Logan, 1986; Reches and Locker, 1994]. In contrast, high porosity sandstone [Aydin and Johnson, 1978; Antonellini and Aydin, 1994] and poorly lithified sands [Mozley and Goodwin, 1995; Sigda et al., 1999; Cashman and Cashman, 2000] deform by cataclasis within deformation bands. Experimental studies have also demonstrated the dependence of mode of deformation on porosity [e.g., Dunn et al., 1973; Wong et al., 1997].

Fractures and deformation bands are hydrologically distinct. In contrast to fractures, deformation bands reduce porosity and saturated permeability with respect to protolith [Antonellini and Aydin, 1994; Sigda et al., 1999; Rawling et al., 2001] and are likely to increase fault unsaturated permeability in the vadose zone of arid desert environments [Sigda and Wilson, 2003].

Previous work in ignimbrite sequences shows that fractures can significantly increase the saturated permeabilities of welded units [Winograd, 1971; Wohletz, 1996; LeCain, 1997]. In this paper, we document a minimum reduction in saturated permeability of deformation bands relative to nonwelded protolith ignimbrite (Bandelier Tuff) using an air-minipermeameter. Backscattered-electron imaging shows that ignimbrite grains are crushed within deformation bands, reducing porosity, pore size, and saturated permeability both normal and parallel to the deformation band. Porosity is reduced by as much as 21% within an unaltered deformation band and up to 43% in

deformation bands containing smectite. Variable pore-size reduction leads to air permeability reduction in the range of one half to one order of magnitude. We note that our measurements likely overestimate fault-zone permeabilities. Hong [1999] demonstrated that water-saturated deformation-band faults in sand that contain smectite, a swelling clay, exhibit an order of magnitude lower permeability than that measured dry. The even smaller decreases in permeability exhibited by the other faults in our study are likely minima also, since most of the deformation-band faults studied were so thin that measurements were influenced by surrounding higher permeability protolith. Other geologic factors influencing the magnitude of permeability reduction in a given fault include local variations in protolith permeability and degree of cataclasis, diagenetic alteration and/or cementation. An unexpected increase in permeability from protolith to deformation band in some cases is attributed to the presence of desiccation cracks and post-cementation fractures in deformation bands containing smectite and calcite, respectively. This effect would not be evident with standard falling-head permeability measurements of smectite-rich faults, as hydration would cause desiccation cracks to close [e.g., Hong, 1999].

Within perched aquifers in the Bandelier Tuff, these lower permeability structures introduce effective permeability heterogeneity and/or anisotropy into the flow field and may affect production of groundwater [e.g., Yobbi, 1997]. If further study shows that the permeability reduction is greater than we have estimated from air-minipermeameter analyses, their impact on saturated flow may be greater. Deformation-band faults may, however, exert the greatest impact on unsaturated flow. Preferential diagenetic

modification of deformation bands is evidence that they have served as preferential fluid flow pathways in the unsaturated vadose zone [Wilson et al., 2003].

Geologic Setting

Our study of pore structure, porosity, and saturated permeability modification within deformation bands was focused on Bandelier Tuff ignimbrite deposits, which are located on the flanks of the Jemez Mountains of northern New Mexico (Fig. 5.2a). The Bandelier Tuff is composed of the lower, 1.6 Ma Otowi Member and the upper, 1.2 Ma Tshirege Member, both of which were deposited from violent pyroclastic eruptions of the Valles/Toledo caldera complex [Smith and Bailey, 1966; Izett and Obradovich, 1994]. Both members are dominated by silicic ash with lesser amounts of pumice, lithic fragments, and phenocrysts of quartz, sanidine, and plagioclase feldspar [Broxton et al., 1995]. The Otowi Member (Qbo) is a single, nonwelded, glassy cooling unit (Fig. 5.2b). The Tshirege Member (Qbt) comprises a sequence of cooling units, which vary in degree of welding and postdepositional crystallization (Fig 5.2b).

These welding and crystallization characteristics are the main petrophysical controls on deformation in ignimbrites, and therefore influence the mode of deformation in each unit [Wilson et al., 2003]. The differentiation among units according to response to fault-zone deformation defines a mechanical stratigraphy for the Bandelier Tuff (Fig. 5.2b), in which the stratigraphic section is dominated by nonwelded ignimbrites that fail by the formation of deformation bands.

On the Pajarito Plateau, the Bandelier Tuff is cut by the Pajarito fault system, a 41-km-long, rift-related, normal fault system consisting of four large faults, each dipping

steeply west or east and striking approximately north (Fig. 5.2a). Displacement is characteristically dip-slip, up to 180 m on the Pajarito fault with local evidence of strike-slip movement [Carter and Gardner, 1995]. Conceptual models of groundwater flow focus on how topography and this large-displacement fault zone affect regional flow paths [e.g., Rogers et al., 1996]. However, many small-displacement faults (mm-m throw) are also present, and may number in the thousands over a km^2 area on the Pajarito Plateau [e.g., Carter and Winter, 1995]. Although rarely mapped because of their size, the spatial distribution and character of these faults are important to understanding both regional deformation and subsurface fluid flow [cf. Sigda et al., 1999].

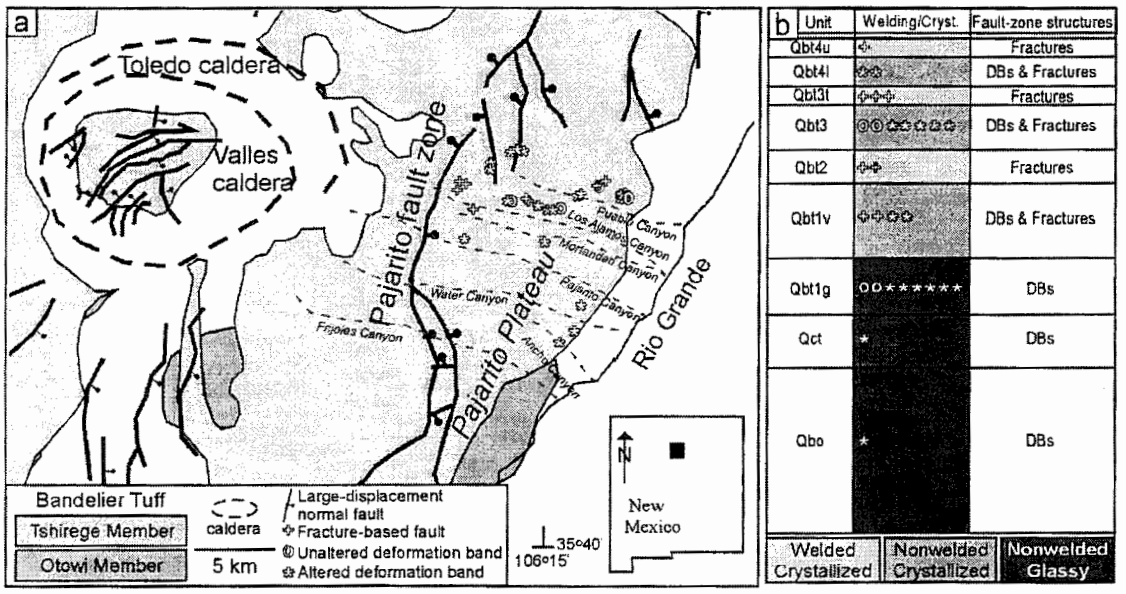

Figure 5.2. (a) Location map modified from Aldrich [1986], Heiken et al. [1990], Purtymun [1995], and Stimac [1996]. Shading shows extent of Bandelier Tuff. Dashed lines give approximate locations and trends of major canyons. (b) Bandelier Tuff stratigraphy of Lewis et al. [2002] modified to highlight mechanical behavior of stratigraphic units [cf. Wilson et al., 2003]. Thicknesses are schematic. Not all units are present in all locations. Symbols show the distribution of different fault types that were studied in detail in map view (a) and stratigraphic position (b). DB's = deformation bands, Qbo = Otowi Member, Bandelier Tuff, Qbt = Tshirege Member, Bandelier Tuff.

The Bandelier Tuff is largely above the water table, and, for the most part has been since deposition [Purtymun and Johansen, 1974]. In the semiarid climate of the Pajarito Plateau, deeply incised canyons trending roughly E-W from higher to lower elevations create two distinct hydrologic regimes: mesa tops and canyon bottoms (Fig. 5.2a) [Rogers et al., 1996]. Canyon bottoms are the dominant sources of recharge to the groundwater regimes beneath the Pajarito Plateau. These groundwater regimes include: (1) the main aquifer within the Puye Conglomerate and Santa Fe Group sediments , (2) shallow alluvium deposited in some large canyons near the Rio Grande River, and (3) discontinuous intermediate layers within the lower, nonwelded portions of the Bandelier Tuff and underlying basalts and sediments (Fig. 5.3) [McLin, 1996]. We focus on how deformation bands may affect saturated flow in the latter of these groundwater regimes.

Saturated flow in the perched aquifers is dominantly eastward toward the Rio Grande. However, small-displacement faults may alter flow paths by either inhibiting or enhancing fluid flow and transport. Fractures, widely recognized as conduits under saturated conditions, are prevalent in the welded units of the Bandelier Tuff and underlying basalts, and therefore fracture-based faults may enhance hydraulic connectivity in these perched aquifers [e.g., Wohletz, 1999]. On the other hand, small-displacement faults in nonwelded ignimbrites and poorly consolidated rift sediments are dominated by deformation bands [e.g., Sigda et al., 1999; Rawling et al., 2001; Wilson et al., 2003]. Studies of deformation bands in sands show that pore size, porosity, and saturated permeability can be drastically reduced relative to protolith, likely inhibiting saturated flow [Sigda et al., 1999]. In this paper, we document modifications in pore size, porosity, and saturated permeability within deformation bands in nonwelded

ignimbrites in order to determine whether these structures could also impact saturated flow and water recovery in the perched aquifers of the Bandelier Tuff [e.g., Rogers et al., 1996; Yobbi, 1997].

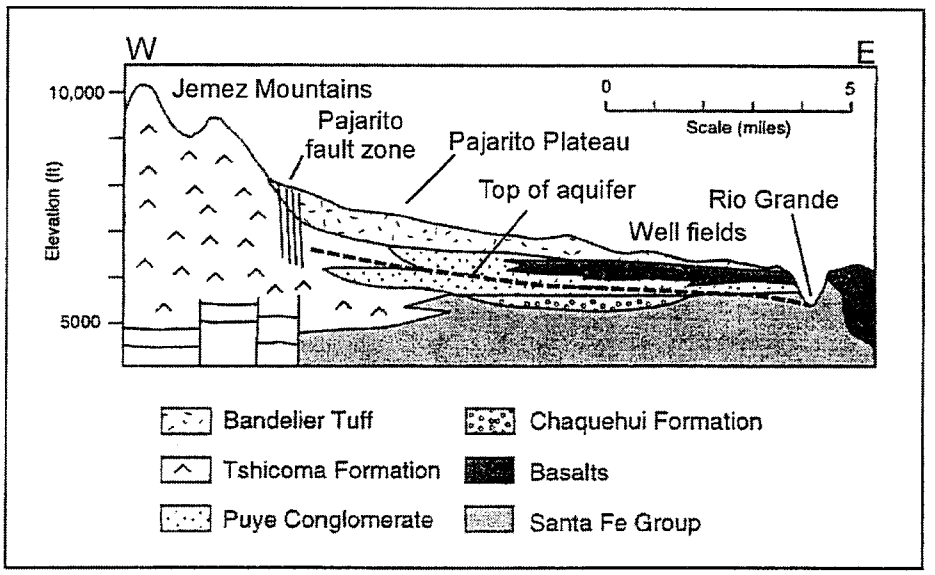

Figure 5.3. Geologic cross section through the Pajarito Plateau showing conceptual sketch of hydrogeologic units and aquifer levels. After Purtymun [1995] and Rogers et al. [1996].

Characteristics of Deformation-Band Faults on the Pajarito Plateau

High porosity and heterogeneous pore structure in poorly sorted, nonwelded ignimbrites are modified by pore collapse and grain-size reduction within deformation bands (Fig 5.1c, d; Fig. 5.4a, b) [Wilson et al., 2003]. Porosity is reduced, pore structure is variably homogenized, and pore connectivity is variably increased by destruction of glass walls that had previously isolated pore spaces (i.e., pumice vesicles).

In the nonwelded ignimbrites of the Bandelier Tuff, zones of deformation bands range in thickness from 1 mm to 15 cm, and contain variable amounts of diagenetic smectite and calcite cement [Wilson et al., 2003]. These minerals are not abundant in surrounding protolith (Chapter 4) and result in significant porosity reduction (Fig. 5.4c,

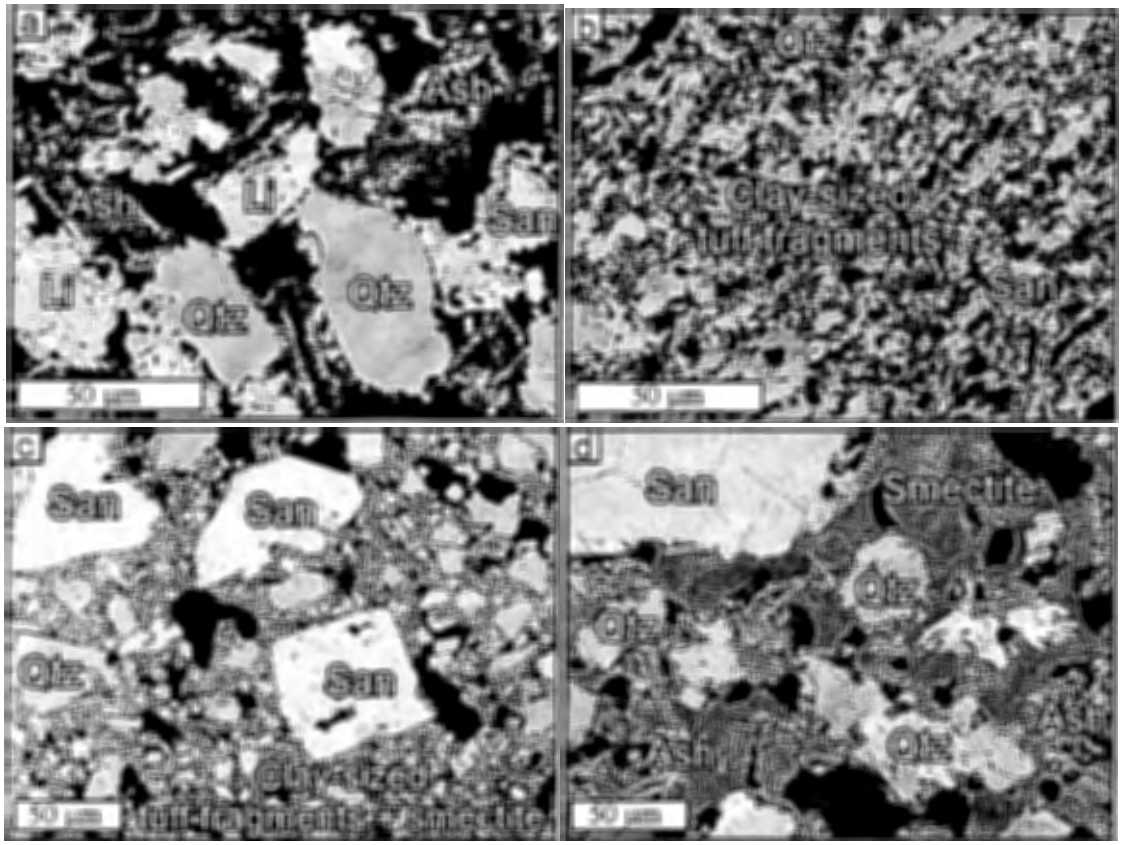

Figure 5.4. BSE images of (a) nonwelded crystallized ignimbrite, (b) unaltered deformation band in which grains are reduced to predominantly clay-sized fragments with highly irregular edges, (c) deformation band with 1.4 wt% smectite, and (d) deformation band with 94 wt% smectite. Qtz = quartz phenocryst, San = sanidine phenocryst. Note that both relative sizes and area of pore spaces (black) decrease from (a) to (c). Sizes of pore spaces appear similar in (c) and (d) due to desiccation cracking and plucking of pure smectite in more clay-rich deformation band (d).

d). Most deformation bands exhibit foliation defined by compositional layering or alignment of grains and/or diagenetic minerals parallel to fault boundaries.

The reduction in pore space and variable increase in pore connectivity within deformation bands in the vadose zone of arid environments results in preferential water retention [Sigda and Wilson, 2003]. In the Bandelier Tuff, this leads to (1) preferential *in situ* alteration of ignimbrite matrix (volcanic glass, feldspar, and mafic lithic clasts) to

smectite, (2) increased infiltration leading to both preferential colloidal transport of smectite (Fig. 5.4c, d) and fault-zone dissolution and/or precipitation, and (3) increased volume of plant roots, playing a key role in calcite cementation in these deformation bands (Chapter 4).

Methods

More than 100 faults in welded and nonwelded ignimbrite units of the Bandelier Tuff were characterized at the outcrop scale (Fig. 5.2; Appendix A). A representative subset of these faults and corresponding protolith was identified for additional detailed study (Table 4.2; Table A3, Appendix A). This subset of faults includes unaltered deformation bands, deformation bands with 1.4 to 93.5 wt% smectite, calcite-cemented deformation bands, and fractured ignimbrite. The relative amounts of pumice, matrix glass, phenocrysts, and lithic fragments were determined for each protolith-fault pair by point counting on a petrographic microscope (Table B1, Appendix B). Porosity was determined in two dimensions by pixel counts of black (porosity) versus gray (grain) within back-scattered electron microprobe images using Matlab (Appendix B). An alternate method of determining three-dimensional, effective porosity was also employed for a subset of protolith samples. The volume, dry mass, and water-saturated mass of ignimbrite protolith were measured, and effective porosity was calculated from these data.

Protolith, fault-parallel and fault-normal saturated permeabilities were measured for protolith-fault pairs in order to determine the hydrologic impact of deformation bands in ignimbrites in perched saturated zones. Sets of permeability data were collected and

organized by date (Appendix C) in order to constrain such conditions as temperature, atmospheric pressure, etc., for a given set of measurements. These measurements were made on samples collected for lab analysis and at outcrop sites with a portable air-minipermeameter based on a design by J. Matt Davis at the University of New Hampshire. This design was chosen because it is ideal for obtaining rapid measurements in both a lab and field (outcrop) setting. In the air-minipermeameter design, air from a compressed air tank enters the air-minipermeameter at a constant pressure, travels through a mass flow meter (rotameter) and a pressure gauge, and then out of the air-minipermeameter through flexible tygon tubing to the tip seal (Fig. C1, Appendix C). Gas is directed into the rock via this tip seal, which consists of a rigid brass housing to which a molded silicone rubber ring is affixed. This soft, durable silicone rubber establishes the seal between the injection nozzle and the rock surface. The tip seal size used for all measurements has a 0.31 cm inner radius and a 0.62 cm outer radius. Similar to Davis et al. [1997], we use the approximation that the radius of influence for this 2:1 outer to inner tip seal radius ratio is 4 times the inner tip seal diameter (Fig. 5.5) [Goggin et al., 1988], and that the permeability measurements represent a hemispherical volume of interrogation with a radius of 2.48 cm. As opposed to a tip seal with a 4:1 ratio, the 2:1 tip seal ratio has a smaller sample volume and can be used to minimize effects of sample boundaries. Since most deformation bands are narrower (typically 1 mm) than the radius of influence (Fig. 5.5), the 2:1 tip seal was chosen to minimize the impact of adjacent protolith on fault permeability measurements; however, we were not able to measure the permeability of deformation bands alone. All permeabilities were calculated

from Darcy's law using the applied pressure, measured flow rate, and the geometry of the tip seal [e.g., Suboor and Heller, 1995].

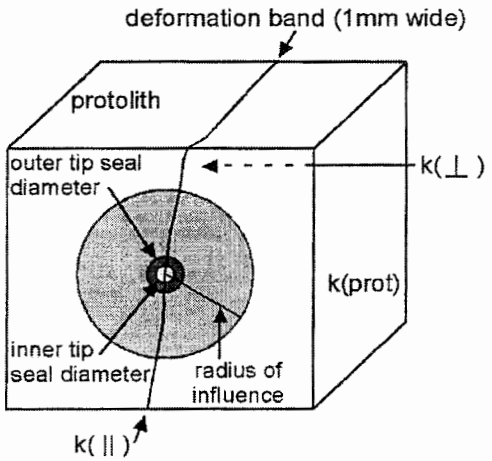

Figure 5.5. Schematic diagram showing measurement location and tip seal coverage for fault-parallel, k (||), permeability measurement. Inner tip seal diameter is 0.62 cm, outer tip seal diameter is 1.24 cm. Radius of influence is 4 times the diameter of inner tip seal (2.48 cm). Fault-normal, k (⊥), and protolith, k (prot), permeability measurement locations are also shown. Fault-normal measurements were taken by removing protolith material to reveal the deformation band.

Standardization

Instrument drift and measurement error were documented by comparing lab or outcrop permeability measurements of standards from one data-collection period to the next. Standards included a suite of ignimbrite and sandstone samples provided by Vince Tidwell at Sandia National Laboratory (SNL). Prior to use in this study, these samples were measured for air permeability with a multisupport permeameter (MSP) at SNL. This MSP is equipped with a pneumatic piston to compress the tip seal to the prepared surface [Tidwell and Wilson, 1997; 1999]. Measurements of standards in this study were

performed periodically before or after a set of protolith-fault measurements in order to document instrument drift and measurement error. Instrument drift refers to the steady increase or decrease in measurement values for a standard with continued minipermeameter use. Measurement error is the standard deviation from the mean of permeability measurements taken for a standard over several dates. These errors were minimized by (1) having a consistent operator for all experiments, (2) shielding the minipermeameter and gas source from extreme cold and heat, and (3) carefully choosing measurement locations on a sample or outcrop that do not lie on major visible heterogeneities.

Results

Evaluation of Approaches to Determining Porosity

Effective porosity determined from sample volume and dry versus saturated mass was found to be consistently higher, averaging approximately 9% greater, than the BSE-image derived, two-dimensional porosity values (Table 5.1). However, poorly lithified protolith and fault samples typically disaggregated upon saturation with water. We therefore rely on BSE image analysis to compare the porosities of faults with protolith. Thus, the porosity values given in this study (discussed in a later section) should be considered minimum values.

Standardization of Saturated Permeability Measurements

Samples of ignimbrite and sandstone were used as standards to check the accuracy of protolith-fault permeability values obtained from the air-minipermeameter. Permeabilities obtained with the MSP were compared to the minipermeameter

measurements of each standard for a given set of protolith-fault data (Table 5.2).

Table 5.1. Comparison of effective porosity determinations for selected ignimbrite protoliths.

Sample#	Volume of dry sample* (cm^3)	Mass of dry sample (g)	Mass of wet sample (g)	Mass of water ^(g)	**Effective porosity~ (%)**	**Porosity from BSE images (%)**	**Difference (%)**
bb3	12.66	30.90	41.27	10.37	47.0	41.0	6.0
bt37	16.10	40.91	56.13	15.22	50.6	46.9	3.7
bt73	14.25	37.66	50.36	12.70	49.1	40.6	8.5
bt109	8.49	22.46	24.97	2.51	24.3	13.1	11.2
bt120	6.02	15.95	23.98	8.03	59.1	42.4	16.7
						Mean difference:	9.2

#Sample numbers correspond to those in Tables 4.2, A1, A3, and A5)

*Volume of sample determined by pichnometer.

^Density of water: $9.23g/10cm^3 = 0.923\ g/cm^3$

~Effective porosity = [(mass of wet sample - mass of dry sample) / density of water] / volume of dry sample

Table 5.2. Air-saturated permeabilities for standards--comparison of MSP versus air-minipermeameter values.

Sample	MSP measurement (m^2)	Minipermeameter measurement (m^2)	Date of minipermeameter measurement
Pink ignimbrite	**4.64E-15**	**6.12E-14**	Mean permeability for dates below
		1.40E-14	Standard Deviation
		5.49E-14	23-Jul-03
		5.39E-14	6-Aug-03
		5.73E-14	6-Aug-03
		5.21E-14	12-Aug-03
		5.98E-14	18-Sep-03
		8.92E-14	18-Sep-03
Orange ignimbrite	**1.90E-14**	**9.35E-14**	Mean permeability for dates below
		4.39E-14	Standard Deviation
		4.98E-14	23-Jul-03
		7.45E-14	6-Aug-03
		6.88E-14	6-Aug-03
		1.46E-13	12-Aug-03
		6.98E-14	18-Sep-03
		1.52E-13	18-Sep-03
Gray ignimbrite	**8.16E-14**	**8.85E-14**	Mean permeability for dates below
		1.44E-14	Standard Deviation
		7.17E-14	23-Jul-03
		1.11E-13	6-Aug-03
		8.14E-14	6-Aug-03
		8.55E-14	12-Aug-03
		8.12E-14	18-Sep-03
		1.00E-13	18-Sep-03
Brown sandstone	**1.04E-12**	**1.37E-13**	Mean permeability for dates below
		2.03E-14	Standard Deviation
		1.19E-13	23-Jul-03
		1.34E-13	6-Aug-03
		1.41E-13	6-Aug-03
		1.10E-13	12-Aug-03
		1.49E-13	18-Sep-03
		1.66E-13	18-Sep-03
Massillon sandstone	**8.45E-12**	**2.38E-12**	Mean permeability for dates below
		2.85E-13	Standard Deviation
		2.28E-12	23-Jul-03
		2.76E-12	6-Aug-03
		2.24E-12	6-Aug-03
		1.99E-12	12-Aug-03
		2.34E-12	18-Sep-03
		2.66E-12	18-Sep-03

Minipermeameter measurements for the ignimbrite standards varied by relatively large amounts, and were variably higher or lower than the MSP permeability values. In contrast, permeability measurements for the sandstone standards were relatively constant and were consistently lower than MSP permeability values. Based on these trends and visual inspection of the standards, the ignimbrite samples were considered too heterogeneous to serve as standards to document instrument drift or measurement error. The more homogeneous brown and Massillon sandstones were more suitable for these purposes. Due to the availability of published permeability data on Massillon sandstone [Tidwell and Wilson, 2000; Lechler, 2002], it was chosen to document instrument drift and measurement error.

The Massillon sandstone dataset obtained with the minipermeameter does not show an overall increasing or decreasing trend (Table 5.2), suggesting that no instrument drift occurred with continued minipermeameter use. However, the average minipermeameter measurement for Massillon sandstone was low, 2.38×10^{-12} m^2 with a standard deviation (measurement error) of 2.84×10^{-13}, compared to the MSP measurement of 8.45×10^{-12} m^2. A correction for the low average permeability measurement for Massillon sandstone was not performed since the primary objective of this study is to document the permeability differences between fault and protolith samples. Thus, relative differences are more important than absolute values. As detailed below, our permeability measurements of Massillon sandstone standard are fairly consistent from one measurement date to the next. This documents the consistency of conditions by which fault and protolith permeability measurements were taken, thus ensuring that permeability differences between protolith and fault are recognized.

Porosity and Permeability Differences for Protolith-Fault Pairs

Porosity is increased by fractures (Fig. 5.1b). As a result, fractures are by far the greatest influence on saturated permeability in welded ignimbrites, increasing permeability by at least two orders of magnitude (Table 5.3; Fig. 5.6). In contrast, deformation bands in nonwelded ignimbrite units are variably diagenetically modified zones of grain crushing and pore collapse (Fig. 5.4). Not surprisingly, they result in porosity and permeability reduction (Table 5.3).

Table 5.3. Porosity & permeability differences between protolith-fault pairs.

Protolith-fault pair	Fault thickness (mm)	Porosity (%)	Normalized* difference in porosity	Fault-parallel k_{sat} (m^2)	Normalized* difference in fault-parallel k_{sat}	Fault-normal ksat (m^2)	Normalized* difference in fault-normal k_{sat}
Crystallized welded ignimbrite (Qbt3t)		10		5.2E-14		5.2E-14	
Fracture	1	100^	10.00	5.4E-12	103.85	NA	NA
Glassy NW ignimbrite (Qbt1g)		56		1.1E-12		1.1E-12	
Unaltered deformation band	1	44	0.79	NA	NA	1.9E-13	0.17
Crystallized NW ignimbrite (Qbt3)		47		6.0E-13		6.0E-13	
Unaltered deformation band	80	26	0.55	1.1E-13	0.18	1.7E-13	0.28
Crystallized NW ignimbrite (Qbt3)		37		1.2E-12		1.2E-12	
Deformation band (1.4 wt% smectite)	10	0.2	0.01	1.6E-12	1.33	8.9E-13	0.74
Glassy NW ignimbrite (Qbt1g)		49		1.1E-12		1.1E-12	
Deformation band (7.8 wt% smectite)	30	19	0.39	NA	NA	3.0E-13	0.27
Glassy NW ignimbrite (Qbt1g)		49		1.1E-12		1.1E-12	
Deformation band (17.4 wt% smectite)	30	13	0.27	6.2E-13	0.56	4.0E-13	0.36
Crystallized NW ignimbrite (Qbt4)		42		4.0E-13		4.0E-13	
Deformation band (93.5 wt% smectite)	1	14	0.33	NA	NA	1.9E-13	0.48
Glassy NW ignimbrite (Qbt1g)		54		4.7E-13		4.7E-13	
Calcite-cemented deformation band	2	11	0.20	7.1E-13	1.51	8.3E-14	0.18

*Normalizations were calculated as average fault value / average protolith value (normalized protolith values = 1; decreases from protolith <1, increases from protolith

^Porosity of fracture only considered, spatial density and aperture of fractures not considered.

NA = not analyzed, NW = nonwelded.

Unaltered deformation bands show moderate reductions in porosity and permeability (Figs. 5.1d and 5.4b; Table 5.3). These deformation bands also have variable thickness, ranging from 1 to 80 mm. Due to the volume of interrogation imposed by our tip seal, permeability measurements of deformation bands thinner than

49.6 mm are likely affected by surrounding, higher permeability protolith, and thus are overestimates of permeability.

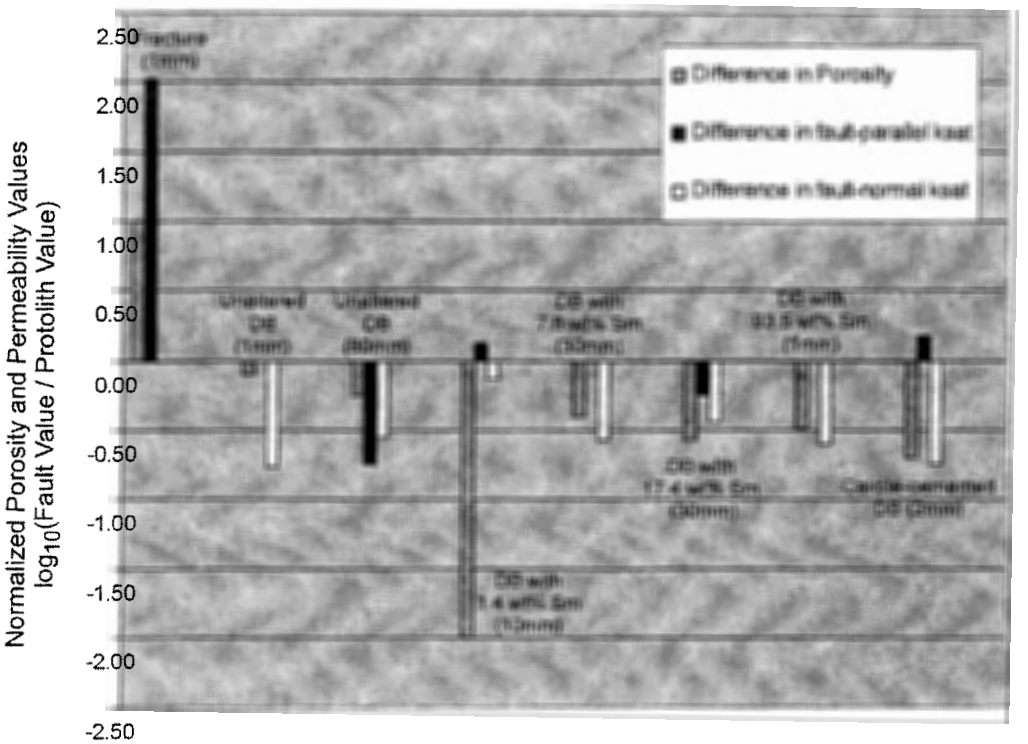

Figure 5.6. Normalized differences in porosity, fault-parallel saturated permeability, and fault-normal saturated permeability for fractures and variably altered deformation bands (DB). Sm = smectite. Thickness of fault is given below each fault description.

Deformation bands containing diagenetic minerals generally show larger reductions in porosity, but variable decreases in saturated permeability (Fig. 5.6). Among the protolith-fault pairs, the largest decreases in permeability are not associated with the highest porosity reductions (Table 5.3; Fig. 5.6). In fact, the largest porosity reductions result in surprisingly small reductions in fault-normal and fault-parallel saturated permeabilities of less than one order of magnitude (Table 5.3; Fig. 5.6). This smaller than expected reduction in permeability is in part due to the thickness of all deformation

bands that contain smectite or calcite. All are narrower than 49.6 mm, which allows higher permeability protolith to be incorporated into the fault-permeability measurement.

Two exceptions to the reduction in saturated permeability from protolith to fault include fault-parallel permeability values of a calcite-cemented deformation band and a deformation band containing 1.4 wt% smectite. These two measurements are up to one half order of magnitude higher than protolith. These increases in air-saturated permeability are likely due to the presence of desiccation cracks and post-cementation fractures, respectively. These structures were not evident in outcrop, but were observed under the petrographic microscope and with BSE imaging.

Permeability Ranges for All Protoliths and Faults

Additional protolith and fault permeability measurements were made on samples that were not analyzed for porosity or diagenetic mineral content. These permeability data (Table C3, Appendix C) are combined with data from Table 5.3 to show the overall ranges in permeability for different types of protolith and fault (Fig. 5.7).

Measured permeabilities of glassy nonwelded protolith range from $10^{-12.4}$ to $10^{-11.9}$ m^2. Crystallized nonwelded protolith permeabilities have a wide range of $10^{-12.9}$ to $10^{-11.3}$ m^2. Permeabilities measured parallel to deformation bands are generally reduced compared to protolith but are typically higher than those measured normal to the deformation band. Fault-normal permeabilities for unaltered deformation bands range from $10^{-13.0}$ to $10^{-12.2}$ m^2 (Fig. 5.7). Fault-parallel permeabilities for unaltered deformation bands show more variability, from $10^{-13.2}$ to $10^{-11.3}$ m^2. Deformation bands containing smectite have permeability ranges similar to both protolith and unaltered deformation

bands. Fault-normal permeabilities range from $10^{-12.9}$ to $10^{-11.9}$ m^2, and fault-parallel permeabilities range from $10^{-12.2}$ to $10^{-11.7}$ m^2. The calcite-cemented deformation band has the lowest fault-normal permeability of $10^{-13.2}$ m^2, and a moderate fault-parallel permeability of $10^{-12.2}$ m^2. Welded ignimbrite is less permeable than nonwelded ignimbrite, ranging in permeability from $10^{-13.3}$ to $10^{-12.3}$ m^2, with fracture-parallel permeabilities ranging from $10^{-11.5}$ to $10^{-11.1}$ m^2.

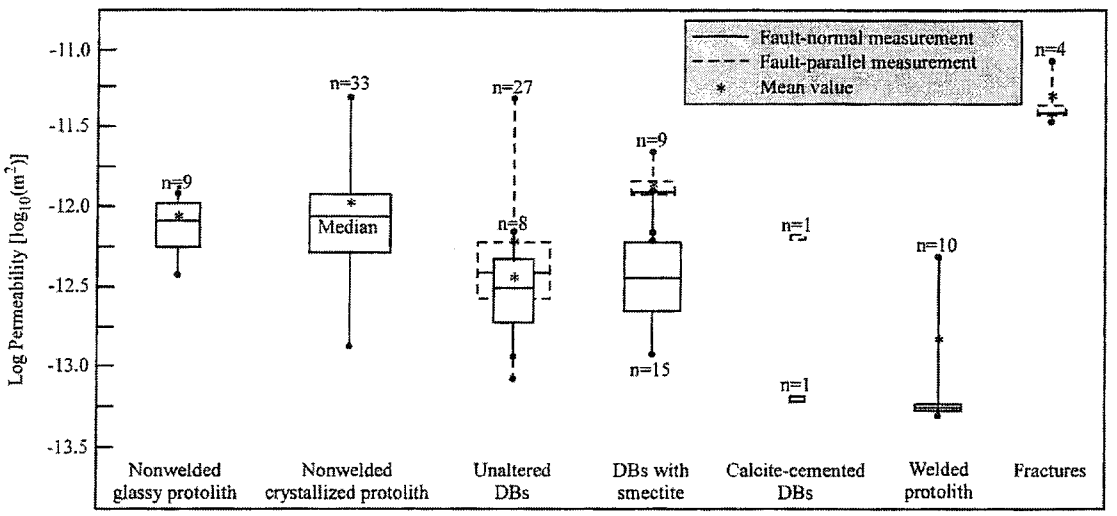

Figure 5.7. Box plots of log saturated permeabilities of protoliths with variable welding and crystallization characteristics, and different fault types (fractures, deformation bands (DBs), and altered and/or mineralized deformation-band fault zones). Data collected *in situ* and on hand samples using an air–minipermeameter. Boxes encompass 50% of data, vertical lines bounded by filled circles show full range of data, horizontal line within each box is the median permeability, asterisks indicate mean permeability, and box widths are proportional to the square root of n for each group.

Discussion

Measurement error

Permeability measurement of Massillon sandstone standard yields a mean permeability of 2.38 x 10^{-12} m^2 with a standard deviation, or measurement error, of 2.85 x

10^{-13}. This is a significant error, potentially caused by biases or small uncertainties in input parameters in permeability calculations, spatial variability of the standard, any miniscule tilt on the tip seal that could alter the radius of influence (Fig. 5.5), and/or differences in mode of measurement (manual versus automated). However, this error is fairly consistent from one measurement date to the next (Table 5.2). This documents the consistency of conditions by which fault and protolith permeability measurements were taken, thus ensuring that permeability differences between protolith and fault are recognized. Therefore, measurement error does not affect our objective of identifying significant permeability modifications (i.e., contrasts of at least two orders of magnitude).

Non-Darcian Flow Effects

Our measurements of permeability for Massillon sandstone were consistently lower than, but within one order of magnitude of, the automated measurement provided by V. Tidwell. This difference in permeability values may be due to sample heterogeneity. Measurement of air permeability on the Massillon sandstone standard with the MSP may have been made in a different location on the sample than that consistently measured with the minipermeameter. Since Massillon sandstone is actually fairly heterogeneous (although less so than ignimbrite), different values in permeability from one location to another in the same sample may cause the small difference in permeability measurement from the MSP to our minipermeameter.

Alternatively, high velocity (inertial) non-Darcian flow effects, which result in pressure losses and an underestimate of permeability [Davis et al., 1994], may be causing the consistently lower permeability measurements. These effects may be accentuated by

the 2:1 tip seal which forces air through a smaller sample volume than a 4:1 tip seal [Lechler, 2002]. Also, at higher gauge pressures, measured flow rates are less than expected for Darcian behavior. A lower flow rate and non-linear deviation from Darcy's law is due to inertial effects resulting from the transition to turbulent gas flow. Deviation from Darcy's law occurs at a gauge pressure of 0.029 to 0.363 psi for Massillon sandstone [Lechler, 2002]. Measurements below these pressures reflect Darcian flow; measurements above these pressures reflect non-Darcian flow and are biased toward lower permeabilities. All measurements in this study were made at gauge pressures that ranged from 0.5 to 15 psi, within the range of non-Darcian flow. Gauge pressures for deformation-band permeability measurements range from 3.4 to 10.6 psi and for protolith from 1.0 to 6.6 psi. Given the similarities in the ranges of these gauge pressures, this effect may be fairly consistent for all measurements. Therefore, our objective of identifying the effect that deformation-band faulting has on permeability may not be significantly affected.

Effect of Deformation-Band Thickness on Fault-Normal Permeability Measurements

For permeability calculations, the material through which air flows is assumed to be relatively homogeneous. However, because fault zones are thin (Fig. 5.6), fault measurements typically encompass two materials with different hydrologic properties. Flow through a wide deformation band fault zone (greater than 4 times the inner tip seal diameter) may be considered homogeneous; flow through a narrow deformation band incorporates the hydrologic properties of surrounding protolith into the permeability calculation.

Deformation-band fault zones analyzed in this study range in width from 1 to 80 mm. The volume of interrogation for narrow deformation-band fault zones (those that are < 49.6 mm wide for a tip seal with an inner diameter of 0.62 cm) can be considered a two-layer system consisting of the deformation-band fault zone and surrounding protolith. Corrections to remove the effect of the surrounding protolith can better isolate the hydrologic properties of the deformation-band fault zone. This involves calculation of a dual versus single layer geometric factor (G_d versus G_o) [Aronson, 1999]. We were not able to evaluate the magnitude of the effect that deformation-band fault zone thickness would have on fault-normal permeability since there were not enough permeability data for wide versus narrow deformation-band fault zones in this study. Additional data collection to document this relationship and constrain data corrections is anticipated.

Uncertainties in Saturated Permeabilities Associated with Smectite and Calcite in Deformation Bands

The small reduction and even local increase in fault permeability for diagenetically modified deformation bands relative to protolith reflects not only the influence of surrounding undeformed protolith, but also: (1) post-cementation fractures in calcite-cemented deformation bands, (2) open desiccation cracks in deformation bands containing smectite, and (3) the use of air instead of water for the saturating medium in an investigation of materials containing swelling clays (e.g., smectite) [Sigda et al., 1999; Hong, 1999]. These effects result in measured fault air-permeabilities that are considered maximum values. Hong [1999], for example, shows an order of magnitude smaller permeability of deformation-band faults in sand measured with a flexible-wall

permeameter than with an air-minipermeameter. Since the faults he examined have far less smectite than some of the faults studied here [Sigda et al., 1999; Wilson et al., 2003], this effect may be more pronounced in this study. Although the magnitude of permeability reduction is not well characterized in this study, we propose that deformation bands containing smectite or calcite are likely to have the largest impact on saturated permeability of the faults examined in this study.

Heterogeneity of Saturated Permeabilities of Protolith Versus Deformation Bands

Given the effects of deformation band thickness and the presence of diagenetic minerals, we use only data from the widest unaltered deformation-band fault zones to evaluate the effect that deformation bands may have on saturated permeability in nonwelded ignimbrites. One fault in this study meets these criteria, with a thickness of 80 mm and absence of smectite or calcite (Fig. 5.4b). This fault exhibits a one half to one order of magnitude decrease in fault-parallel and fault-normal permeability. However, comparison of this permeability modification to the wide range in values for unfaulted ignimbrite (just over two orders of magnitude; Fig. 5.7) reveals that the impact of unaltered deformation bands on saturated flow may be minimal.

Implications for Saturated Flow Through Nonwelded Ignimbrites

The reduction in saturated permeability of unaltered deformation bands relative to protolith is similar, at least in process, to the porosity and permeability reductions observed in high porosity sandstones and sands [Antonellini and Aydin, 1994; Sigda et al., 1999]. Porosity within sandstone may decrease from a value of 25% down to 1%,

and permeability from more than 10^{-13} to less than 10^{-15} m^2 [Antonellini and Aydin, 1994]. Reductions of up to three orders of magnitude in air-saturated permeability for deformation bands containing relatively small amounts of clay (< 30 %) have also been documented in poorly lithified sands [Sigda et al., 1999]. Additional water-saturated permeability measurements performed on these same faults demonstrated that faults containing swelling clay (smectite) exhibited permeabilities up to four orders of magnitude lower than adjacent sand [Hong, 1999]. In these faults, adding water caused the clays to swell, further blocking porosity and reducing permeability [Hong, 1999]. This suggests that deformation bands in sands and sandstones, in sufficient numbers, can inhibit cross-fault saturated flow, especially where the faults contain even small amounts of smectite.

In ignimbrites, deformation bands show similar reductions in porosity, but air-saturated permeability is reduced by only one order of magnitude at most. The reduction in saturated permeability for unaltered deformation bands relative to protolith is small, and may only have the effect of creating small permeability heterogeneities in the perched aquifers beneath the Pajarito Plateau. However, the number of unmapped, small-displacement faults can be very large in this tectonically active area of rift extension, on the order of 3000 within a roughly 400-km^2 area [Carter and Winter, 1995]. Although a systematic study of deformation-band fault spatial densities on the Pajarito Plateau has not yet been done, direct observations of deformation bands in nonwelded portions of the Bandelier Tuff suggest that deformation-band faults are likely to be distributed in these deposits at a regional scale. Of these deformation-band faults, the majority contain some amount of smectite, ranging from 1.4 to 93.5 wt%. Given the size of the volume of

interrogation relative to the size of the deformation bands during permeability measurements, and the potential effect of smectite on air- versus water-saturated permeability measurements on dry fault material, smectite-rich deformation band permeabilities are likely to be two orders of magnitude or more lower than the protolith. Therefore, they are likely to have the largest impact on saturated permeability of the faults examined.

The differences between the fault-normal and fault-parallel saturated permeabilities of deformation bands documented in this study suggest permeability anisotropy within the faults themselves (i.e., at the mm scale). At the scale of a perched aquifer (m to km scale), an accurate characterization of permeability anisotropy would have to take into account these direction-dependent permeability variations of deformation bands as well as their thicknesses, spatial density, distribution, and orientations [cf. Antonellini and Aydin, 1994; cf. Yobbi, 1997]. Although the petrophysical properties of deformation-band faults have been documented [Wilson et al., 2003], refinement of permeability values and a comprehensive geometric characterization of deformation-band faults across the Pajarito Plateau must be performed in order to evaluate the effect that these faults may have on saturated flow and water production at the aquifer scale.

Ultimately, deformation-band faults in the Bandelier Tuff may have the most effect on unsaturated, vadose-zone flow since these deposits lie mostly above the regional groundwater table and are saturated only within discontinuous perched aquifers [cf. Purtymun and Johansen, 1974; cf. McLin, 1996]. Current models of vadose-zone fluid flow through ignimbrites only consider fractures in welded units as significant flow

pathways [e.g., Turin and Rosenberg, 1996; Wolfsberg et al., 2000] (cf. Fig. 4.19, Chapter 4). However, the diagenetic record of preferential fault-zone alteration and cementation suggests that deformation bands in nonwelded units may also be fluid flow conduits above the water table [Wilson et al., 2003]. The indirect result on saturated flow is that the preferential vadose-zone fluid flow through these deformation bands and the potential for enhanced transport may affect the amount and chemistry of fluids that end up in both the regional and perched aquifers that underlie the Pajarito Plateau.

Conclusions

In the ash-dominated ignimbrites of the Bandelier Tuff, New Mexico, welded units deform by fracture, and nonwelded glassy units deform by cataclasis within deformation bands [Wilson et al., 2003]. Analysis of BSE images from protolith and deformation-band fault material shows that cataclasis within deformation bands reduces porosity via grain- and pore-size reduction by up to 21%. In the vadose zone of dry environments, this porosity reduction leads to preferential fluid flow and diagenesis [Wilson et al., 2003; Chapter 4), further reducing porosity and pore sizes. Therefore, deformation bands have very different hydrologic properties than fractures. Fracturing within welded units significantly increases porosity and pore connectivity, resulting in an increase in saturated permeability of at least two orders of magnitude. In contrast, we show that deformation bands are zones of reduced saturated permeability. The reduction in saturated permeability compared to protolith, in some cases up to one order of magnitude, could result in permeability heterogeneity and/or anisotropy in nonwelded ignimbrites. Consideration of the limitations in measuring air-saturated permeabilities of

dry, thin deformation bands containing variable amounts of desiccated smectite and fractured calcite cement leads us to propose that the permeability reduction for these faults is likely to be greater by at least an order of magnitude than measured in this study. Therefore, deformation bands, if sufficiently numerous and continuous, may impact fluid flow associated with water recovery [cf. Yobbi, 1997] in perched aquifers across the Pajarito Plateau.

Acknowledgments

This research has been funded by a grant through the Institute of Geophysics and Planetary Physics (IGPP) at Los Alamos National Laboratory. Additional funding was provided by the New Mexico Geological Society. Special thanks to J. Matt Davis for allowing us to replicate his air-minipermeameter and to Floyd Hewitt for construction of the minipermeameter. Thanks to Mark Cal and Justin Prien for assistance in calibrating flow meters, Bob Svec for assistance in calibrating pressure gauges, Vince Tidwell for the use of tuff and sandstone standards, and the New Mexico Firefighter Training Academy for use of compressed air tanks. Also, thanks to Nelia Dunbar and Lynn Heizler for assistance on the electron microprobe, Emily Schultz and Teryn Ebert for assistance in the field, and members of the Faults and Fluids group at New Mexico Tech for many useful discussions.

References

Aldrich, M. (1986), Tectonics of the Jemez Lineament in the Jemez Mountains and Rio Grande rift, *J. Geophys. Res.*, *91*(B2), 1753-1762.

Antonellini, M., and A. Aydin (1994), Effect of faulting on fluid flow in porous sandstones: petrophysical properties, *AAPG Bull.*, *78*, 355-377.

Aronson, E. C., (1999), Modeling investigations on gas permeameters: spatial weighting functions and layered systems, M.S. Thesis, 91 pp., New Mexico Tech, Socorro.

Aydin, A., and A. Johnson (1978), Development of faults as zones of deformation bands and as slip surfaces in sandstones, *PAGEOPH, 116*, 931-942.

Broxton, D., G. Heiken, S. J. Chipera, and F. M. Byers (1995), Stratigraphy, petrography, and mineralogy of Bandelier Tuff and Cerro Toledo deposits, in *Earth Science Investigations for Environmental Restoration—Los Alamos National Laboratory Technical Area 21*, edited by D.E. Broxton and P.G. Eller, Los Alamos National Laboratory Report LA-12934-MS, p. 33-64.

Caine, J. S., J. P. Evans, and C. B. Forster (1996), Fault zone architecture and permeability structure, *Geology*, *24*(11), 1025-1028.

Carter, K. E., and J. N. Gardner (1995), Quaternary Fault Kinematics in the Northwestern Espanola Basin, Rio Grande Rift, New Mexico, *NMGS Guidebook, 46th Field Conference, Geology of the Santa Fe Region*, p. 97-102.

Carter, K. E., and C. L. Winter (1995), Fractal nature and scaling of normal faults in the Espanola Basin, Rio Grande rift, New Mexico: implications for fault growth and brittle strain, *J. of Struct, Geol., 17*(6), 863-873.

Cashman, S., and K. Cashman (2000), Cataclasis and deformation-band formation in unconsolidated marine terrace sand, Humboldt County, California, *Geology*, *28(*2), 111-114.

Chester, F. and J. Logan (1986), Implications for mechanical properties of brittle faults from observations of the Punchbowl fault zone, California, *PAGEOPH, 124*, 79–106.

Davis, J. M., J. L. Wilson, and F. M. Phillips (1994), A portable air-minipermeameter for rapid i*n situ* field measurements, *Ground Water, 32*(2), 258-266.

Davis, J. M., J. L. Wilson, F. M. Phillips, and M. B. Gotkowitz (1997), Relationship between fluvial bounding surfaces and the permeability correlation structure, *Water Res. Res., 33*(8), 1843-1854.

Dunn, D. E., L. J. LaFountain, and R .E. Jackson (1973), Porosity dependence and mechanism of brittle fracture in sandstones, *J.Geophys. Res., 78*(14), 2403-2417.

Goggin, D. J., R. L. Thrasher, and L. W. Lake (1988), A theoretical and experimental analysis of minipermeameter response including gas slippage and high velocity flow effects, *In Situ, 12*, 79-116.

Heiken, G., F. Goff, J. Gardner, W. Baldridge, J. Hulen, D. Nielson, and D. Vaniman (1990), The Valles/Toledo Caldera Complex, Jemez Volcanic Field, New Mexico, *Ann. Rev. Earth Plan. Sci., 18*, 27-53.

Hong, S. -H. (1999) Anisotropic hydraulic conductivity of faulted poorly consolidated eolian sands: Bosque, New Mexico, M.S. Thesis, 70 pp. New Mexico Tech, Socorro, New Mexico.

Istok, J. D., C. A. Rautman, L. E. Flint, and A. L. Flint (1994), Spatial variability in hydrologic properties of a volcanic tuff, *Ground Water, 32*(5), 751-760.

Izett, G. A., and J. D. Obradovich (1994), $^{40}Ar/^{39}Ar$ age constraints on the Jaramillo Normal Subchron and the Matuyama-Bruhnes geomagnetic boundary, *J. Geophys. Res., 99*(B2), 2925-2934.

Knipe, R. J. (1993), The influence of fault zone processes and diagenesis on fluid flow, in *Diagenesis and Basin Development, AAPG, Studies in Geology #36*, edited by A. D. Horbury and A. G. Robinson, eds., pp. 135-148.

LeCain, G. D. (1997), Air-injection testing in vertical boreholes in welded and nonwelded tuff, Yucca Mountain, Nevada, *U.S.G.S. Wat. Res. Inv. Rep. 96-4262*, 33 pp.

Lechler, B.J., 2002, Gas Permeameters: Operation, Modification, and Design, M.S. Thesis, 119 pp., New Mexico Tech, Socorro, New Mexico.

Lewis, C. J., A. Lavine, S. L. Reneau, J. N. Gardner, R. Channell, and C. W. Criswell (2002), Geology of the Western Part of Los Alamos National Laboratory (TA-3 to TA-16), Rio Grande Rift, New Mexico, *Los Alamos National Laboratory Report LA-13960-MS*, 97 pp.

McLin, S. G. (1996), Analysis of water level fluctuation in Pajarito Plateau wells, in, *The Jemez Mountains Region: New Mexico Geological Society 47th Annual Field Conference Guidebook*, edited by F. Goff et al., pp. 421-426.

Mozley, P. S., and L. B. Goodwin (1995), Patterns of cementation along a Cenozoic normal fault: A record of paleoflow orientations, *Geology, 23*, 539-542.

Neeper, D.A., Gilkeson, R.H., 1996, The influence of topography, stratigraphy, and barometric venting on the hydrology of unsaturated Bandelier Tuff, in *The Jemez Mountains Region, New Mexico Geological Society 47th Annual Field Conference Guidebook*, edited by F. Goff et al., pp. 427-432.

Purtymun, W. D. (1995), Geologic and hydrologic records of observation wells, test holes, test wells, supply wells, springs, and surface water stations in the Los Alamos area, *Los Alamos National Laboratory Report LA-12883-MS*, 339 pp.

Purtymun, W. D., and S. Johansen (1974), General geohydrology of the Pajarito Plateau, in *New Mexico Geological Society guidebook, 25th Field Conference, Ghost Ranch*, pp. 347-349.

Rawling, G. C., L. B. Goodwin, and J. L. Wilson (2001), Internal architecture, permeability structure, and hydrologic significance of contrasting fault-zone types, *Geology*, *29*(1), 43-46.

Reches, Z., and D. A. Lockner (1994). Nucleation and growth of faults in brittle rock. *J. Geophys. Res. 99*, 18159-18173.

Rogers, D., and B. M. Gallaher (1995), The unsaturated hydraulic characteristics of the Bandelier Tuff, *Los Alamos National Laboratory Report LA-12968-MS*, 76 pp.

Rogers, D. B., A. K. Stoker, S. G. McLin, and B. M. Gallaher (1996), Recharge to the Pajarito Plateau regional aquifer system, in *The Jemez Mountains Region: New Mexico Geological Society 47th Annual Field Conference Guidebook*, edited by F. Goff et al., pp. 407-412.

Sigda, J. M., L. B. Goodwin, P. S. Mozley, and J. L. Wilson (1999), Permeability alteration in small-displacement faults in poorly consolidated sediments: Rio Grande Rift, central New Mexico, in *Faults and Subsurface Fluid Flow in the Shallow Crust, AGU Monograph 113*, edited by W.C. Haneberg et al., pp. 51-68.

Sigda, J. M., and J. L. Wilson (2003), Are faults preferential flow paths through semi-arid and arid vadose zones?, *Water Res. Res., 39*, doi:10.1029/2002WR001406.

Smith, R. L., and R. A. Bailey (1966), The Bandelier Tuff-A study of ash-flow eruption cycles from zoned magma chambers, *Bull. Volc., 29*, 83-104.

Springer, E. P., and T. G. Schofield (2002), Unsaturated zone hydrologic properties for TA-49, *Los Alamos National Laboratory Report LA-UR-02-6321*, 42 pp.

Stimac, J. A. (1996), Hornbelnde-dacite pumice in the Tshirege Member of the Bandelier Tuff: implications for magma chamber and eruptive processes, in *The Jemez Mountains Region: New Mexico Geological Society 47th Annual Field Conference Guidebook*, edited by F. Goff et al., pp. 269-274.

Suboor, M. A., and J. P. Heller (1995), Minipermeameter characteristics critical to its use, *In Situ*, *19*(3), 225-248.

Tidwell, V. C., and J. L. Wilson (2000), Heterogeneity, permeability patterns, and permeability upscaling: physical characterization of a block of Massillon sandstone exhibiting nested scales of heterogeneity, *SPE Res. Eval. Eng., 3*(4), 283-291.

Tidwell, V. C., and J. L. Wilson (1999), Upscaling experiments conducted on a block of volcanic tuff: Results for a bimodal permeability distribution, *Water Res. Res., 35*(11), 3375-3387.

Tidwell, V. C., and J. L. Wilson (1997), Laboratory method for investigation permeability upscaling, *Water Res. Res., 33*(7), 1607-1616.

Turin, H. J., and N. D. Rosenberg (1996), A conceptual model for flow in the vadose zone beneath the finger mesas of the Pajarito Plateau, in *The Jemez Mountains Region: New Mexico Geological Society 47th Annual Field Conference*, edited by F. Goff et al., pp. 74-76.

Wilson, J. E., L. B. Goodwin, and C. J. Lewis (2003). Deformation bands in nonwelded ignimbrites: Petrophysical controls on fault-zone deformation and evidence of preferential fluid flow, *Geology*, *31*(10), 837-840.

Winograd, I. J. (1971), Hydrogeology of Ash Flow Tuff: A Preliminary Statement, *Water Res. Res., 7*(4), 994-1006.

Winograd, I. J., and W. Thordarson (1975), Hydrogeologic and hydrochemical framework, south-central Great Basin, Nevada-California, with special reference to the Nevada Test Site, *USGS Prof. Pap. 712-C*, 126 pp.

Wohletz, K., 1996, Fracture Characterization of the Bandelier Tuff in OU-1098 (TA-2 and TA-41), *Los Alamos National Laboratory Report LA-13194-MS.*

Wohletz, K. (1999), Fractures in welded tuff, *Los Alamos National Laboratory Report, LA-UR-99-6556*, 27 pp.

Wolfsberg, A., K. Campbell, and J. Fabryka-Martin (2000), Use of chlorine-36 to evaluate fracture flow and transport models at Yucca Mountain, Nevada, in *Dynamics of Fluids in Fractured Rock*, AGU Monograph 122, edited by B. Faybishenko et al., pp. 346-362.

Wong, T.-F., C. David, and W. Zhu (1997), The transition from brittle faulting to cataclastic flow in porous sandstones: Mechanical deformation, *J. Geophys. Res., 102*, 3009–3025.

Yobbi, D. K. (1997), Simulation of Subsurface Storage and Recovery of Effluent Using Multiple Wells, St. Petersburg, Florida, *USGS Water Res. Inv. Rep. 97-4024*, 30 pp.